JSST
Journal of Space Science & Technology

Vol. 8/ No. 4/ Winter 2016
pp. 35-44

Optimal Control of a Tri-axial Spacecraft Simulator Test bed Actuated by Reaction Wheels

H. Taei[1*], M. Mirshams[2], M. Ghobadi[3], M. Amin Vahid D.[4] and H. Haghi[4]

1. Department of Aerospace Engineering, Malek Ashtar University of Technology
2. Department of Aerospace Engineering, K. N. Toosi University of Technology
3. Callege of Engineering, University of Tehran
4. Space Research Lab, K. N. Toosi University of Technology

[*]Postal Code: 158751774, Tehran, IRAN

taei@mut.ac.ir

This article describes the details of a Tri-axial Spacecraft Simulator Testbed (TSST) that has been developed as part of a research program on spacecraft multi-body rotational dynamics and control in Space Research Laboratory (SRL) at K. N. Toosi University of Technology. This dumbbell style simulator includes a variety of components: spherical air-bearing, inertial measurement unit (IMU), rechargeable battery, reaction wheels (RW), on-board computer (OBC) and balancing masses. In this paper, an attitude control problem for the spacecraft simulator actuated by three reaction wheels is studied. Under the assumption of uniform gravity and frictionless air-bearing environment, reaction wheels generate control moments about the roll, pitch and yaw axes of the base body. The control objective is to perform attitude commands sent from users with the least power consumption and a high precision. To handle the non-linear model, a Linear Quadratic Ricatti (LQR) controller has been programmed and it efficaciously controlled the computer-modeled simulator for any given slewing maneuver. This control approach has been developed to facilitate the system to accomplish large-angle, three-axis slewing maneuvers using RWs as effective actuators.

Keywords: spacecraft simulator, air-bearing, reaction wheel, LQR.

Nomenclature

Ψ	Yaw angle
θ	Pitch angle
ϕ	Roll angle
$\vec{\omega}$	Body rates
I	Moment of inertia
$\vec{M}$	Torque
$\dot{\Omega}$	Rotational acceleration of RW
e	Error signal
u	Control effort
T	Total time
J	Performance index
F	Objective function
N	Number of predefined maneuvers
R	Rotation matrix

1. Assistant Professor (Corresponding Author)
2. Associate Professor
3. Ph.D. Student
4. M.Sc.

Introduction

One major aspect that has typically been missing in the area of spacecraft attitude control development is the experimental validation of the available theoretical results. Experimental testing is essential before any novel control laws can be incorporated into future-generation spacecraft [1]. One option to address the problem of unknown uncertainties in ACS testing is to use a hardware-in-the-loop (HIL) experiment by air-bearing simulators. Air-bearing simulators are one of the most common devices used in spacecraft attitude dynamics and control research, because (ideally) they provide unconstrained rotational motion [2-4].

Air-bearing offers a nearly frictionless and torque-free environment, perhaps as close as possible to that of the space, for this reason it is the preferred technology for ground-based research in space dynamics and attitude control, however, it certainly cannot provide the full experience in micro-gravity [5].

Received: 2014. 09.21, Accepted: 2016. 01. 13

Several sophisticated government laboratories and academic institutions have constructed realistic spacecraft simulators that can be used in ground-based experiments and educate the next generation of spacecraft dynamics and control engineers, for example the experiments at: Honeywell, Virginia Polytechnic Institute and State University, University of Michigan, Georgia Institute of Technology, Institute Of Geography (UNAM), M. A. University of Technology, Naval Postgraduate School, etc. [1-15].

The mentioned spacecraft simulator testbed shown in Fig. 1, is a laboratory-based testbed that has been manufactured by SRL to study the concepts of spacecraft attitude dynamics and control. This facility is also used to exhibit the fundamentals of attitude dynamics, spacecraft operational environment, and control to students and experts at K. N. Toosi University of Technology.

Hence, the organization of the paper is as follows. In Section 2, an overview of the TSST hardware and its subsystems is presented. In Section 3, the fundamentals of TSST are described to derive a dynamic modeling for computer-based simulation of TSST attitude motion. Section 4 explains LQR controller and its results in TSST and lastly, Section 5, outlines the conclusion and investigation of the results.

Fig. 1. Tri-axial Spacecraft Simulator testbed (TSST) at SRL

System Overview Spherical Air-Bearing

The tri-axial air-bearing is based on a spherical air-bearing manufactured by SRL. The 220 mm diameter aluminum sphere floats on a thin film of air which exits from holes located on the surface of the cup. This layer of air is an effective lubricant and thus, the environment can simulate operations of satellite or spacecraft.

Compressed air is supplied by means of a compressor with 12 bar capacity. The cup has 13 holes that the compressed air passes them. In this experimental simulator, friction coefficient between the sphere and cup must approximately be equal to zero, and thus the holes combination in cup is very important in the air-bearing design process. For the best design, fluid analysis of air layer should be established, but if designers try to reduce air jets diameter and level the stand, sphere floating will occur in a better form. A pressure regulator has been used to fix the air pressure on the cup surface, too. A one-piece 800 mm stainless steel shaft passes through the center of the sphere and extends between the two octangle mounting plates. Two mounting plates are made from 6.5 mm thick aluminum alloy with 4 holes tapped in a 50 mm grid.

This air-bearing provides unrestricted motion in yaw (rotation about vertical axis) and roll (rotation about the shaft axis). The shaft and plates allow ±25° pitch (rotation about a horizontal axis).

Attitude Sensor

To implement applicable attitude maneuvers by SADS, measurements for the Euler an angles (or quaternions) and the angular rates are required. An inertial measurement unit (IMU) by Micro Strain Inc. was chosen as the attitude sensor unit; because of its simplicity in use, light mass, and low cost. This IMU utilizes the tri-axial gyros to track dynamic orientation and the tri-axial DC accelerometers along with the tri-axial magnetometers to track the static orientation. The embedded microprocessor contains a unique programmable filter algorithm, which blends these static and dynamic responses in real time. This provides a fast response in the face of vibration and rapid movement while eliminating drift. The stabilized output is provided in an easy-to-use digital format. Analog output voltages proportional to the Euler angles can be ordered as an option. Operating over the full 360 degrees of angular motion on all three axes, this IMU provides orientation in matrix, quaternion, and Euler formats.

Table 1. Main Specifications of IMU

Specification	Value
Rotation Boundary	360° (All axes)
Accuracy (Static)	±0.5°
Accuracy (Dynamic)	±2°
Repeatability	0.2°
Operational Voltage	5.2 – 12 VDC
Operational Current	65 mA
Dimensions	64 × 90 × 25 mm
Mass	75 g

Command Computer (User Interface Software)

Users are allowed to command the system by an external desktop computer. This computer communicates directly with OBC via a wireless network device. Also, one of the most useful capabilities of desktop PC is real-time monitoring of all events occurred during the motion of TSST by SATSIM software developed in SRL. With this software, students or other users are able to command TSST for desired motion and observe the sensor outputs, angular velocity of reaction wheels, change of battery capacity and coefficients of control algorithm. If we have several users or students, we can use several computers as command PCs (Fig. 2).

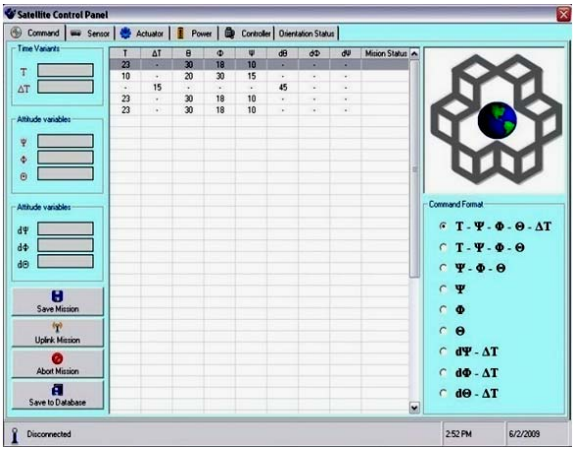

Fig. 2. User interface software (SATSIM)

Reaction Wheels

For control actuation, three reaction wheels have been developed in SRL. These 250 mm diameter reaction wheels are aligned along the yaw, pitch and roll axes for attitude control of TSST. The wheels have been made of two alloys: aluminum and phosphor-bronze. Each reaction wheel is based on a 30 V and 100 Watt DC motor with 3000 rpm capacity as maximum speed. Because of battery limitations, this motor allows 2200 rpm in the highest angular velocity. Each motor has a hall-effect encoder by 120 pulses/revolution capacity for detecting the angular velocity of wheels. One of the most complicated challenges in the reaction wheel construction process is driver development. We designed and manufactured three drivers that can provide the desired angular velocity for each motor. Three points should be considered in driver design: driver communication with on-board processor, angular velocity controlling and encoder connection. Whereas the motors work in 22 V and 100 Watt, the current at starting point would be approximately 5 A, thus drivers should have enough capability to pass this high current. With consideration of these limitations and requirements, an IC based on BTS780 model was selected for drivers. For applying angular velocity commanded by on-board processor to each motor, a micro-controller from AVR family, the ATMEGA32 model, was located in the driver's board, because this micro-controller has high-speed processing procedure and specific outputs for PWM. A CPLD developed by Xilinx co. was selected for computing angular velocity of wheels by using encoders output, too. Each driver can communicate with on-board processor via RS485 serial port (Fig. 3).

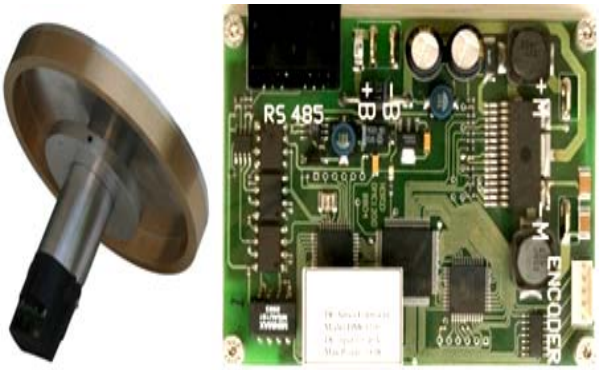

Fig. 3. A reaction wheel and its driver

Table 2. Main Specifications of RWs

Parameter	Value
Angular Momentum (N.m.sec)	7.40
Nominal Rotation Speed (rpm)	3000
Max. Rotation Speed (rpm)	2500
Nominal Torque (N.m)	0.9
Mass (kg)	< 4.3
Moment of Inertia ($kg.m^2$)	0.0282
Operating Voltage (V)	16 - 26

On-board Computer

On-board processor (Fig. 4) is directly the heart of every controllable device, thus development of an effective computer that can process all inputs of control algorithm and command other subsystems is very important and time-consuming. Angular velocity of reaction wheels, system attitude measured by sensor, and change of battery charge are inputs of the control scenario. The main tasks of the central controller are attitude control of TSST, energy management and creating an effective

connection with the external PC. The controller receives commands from SATSIM software via wireless connection and guides TSST to the desired position by using feed-back signal coming from attitude sensor. Processing the encoders and sensor outputs are performed in the on-board computer and commands are finally transmitted to reaction wheels. Yet, central controller should be able to divide the electrical energy between all of the subsystems and display the charge of battery or batteries for users (Fig. 5).

Power Subsystem (Battery)

If we do not have enough electrical energy to handle the simulator subsystems in the duration of each experiment, actually completing the usage of TSST would not be possible. Battery must have enough capacity for maximum energy-consumption instance. This time usually occurs in the starting point of reaction wheels. A Lithium-Polymer battery has been selected for this spacecraft simulator, because this type of battery has such specifications:

a) High efficiency

b) Simple recharge process

c) Low-mass and low-volume

d) Continuous power

e) High safety factor

This battery has been manufactured by Dual Sky and has 5000 mAh, 22 VDC power. Figure represents the overview of the interconnections between TSST components.

Equations of Motion

Equations that characterize the TSST dynamic are represented by a set of coupling differential equations. The rotation of TSST about its three body-fixed axes requires a complex set of torque functions to be applied to the propulsive actuators.

To achieve a generic model of TSST dynamics, the attitude of TSST needs to be described for its three degrees of freedom (rotation about three orthogonal body axes), so frames of reference have to be established. The inertial reference frame establishes a guide for observations of TSST. A logical frame for TSST is earth-fixed. This frame is described using three axes, X, Y and Z, to represent the positive orthogonal unit vectors of the frame. The Z axis points up in the local vertical. The X and Y vectors are perpendicular to this axis and each other, forming an orthogonal, right-handed coordinate set. The orientation of this set about the Z axis is arbitrary, thus it will be assumed that the inertial frame will be aligned with the body frame, described below, in the beginning of each experiment.

Fig. 4. On-board processor

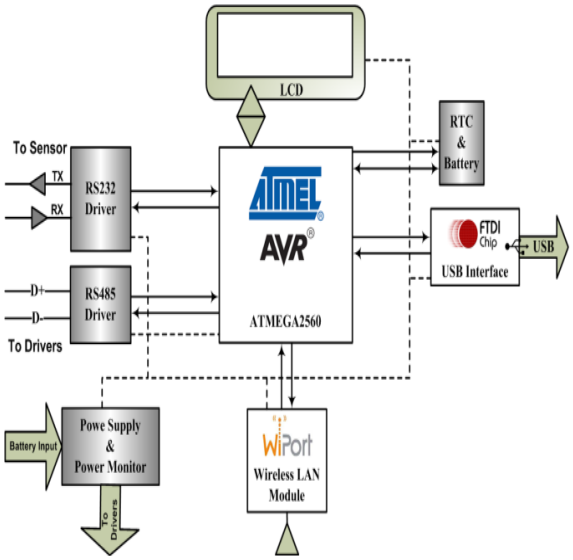

Fig. 5. Block diagram of on-board processor

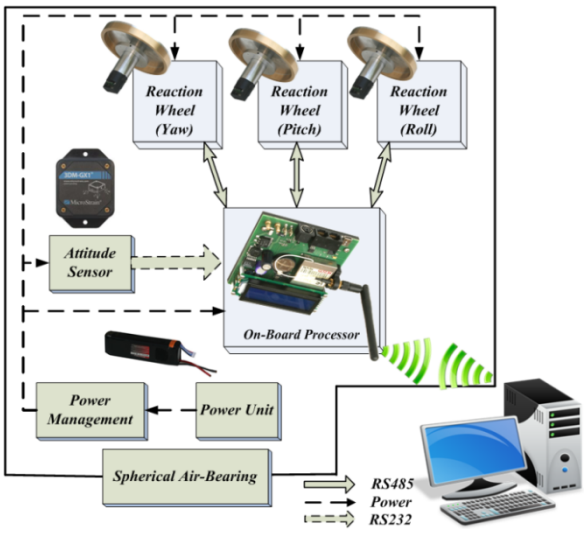

Fig. 6. Overview of the interconnections between TSST components

The body frame is described by the unit vectors x, y and z. physically matching TSST to the body frame; the x axis is selected to be its long axis. The side, perpendicular to the top, is considered the front of TSST. The y axis is chosen to be an axis perpendicular to the long x axis that extended from the center of the sphere toward the front of TSST. The z axis extends from the center of the sphere and extends toward the up plane, perpendicular to it. These three axes constitute a right-handed orthogonal set. Euler $\psi - \theta - \varphi$ orientation angles are chosen to represent simulator attitude, but we should note that its range of motion would be restricted and the maximum angle can reach 25 degrees. To translate data between the body and inertial frames, it is essential to identify rotation matrix for TSST (equation 1).

$$R_{ib} = \begin{bmatrix} c\psi c\theta & s\psi s\theta & -s\theta \\ c\psi s\theta s\varphi - s\psi c\varphi & c\psi c\varphi + s\psi s\theta s\varphi & c\theta s\varphi \\ c\psi c\varphi s\theta & s\psi s\theta c\varphi & c\theta c\varphi \end{bmatrix} \quad (1)$$

where *c* and *s* denote *cos* and *sin*, respectively [16]. The rotation matrix given, if multiplied by the inertial frame coordinated, will give the body frame coordinates. Next, it is essential to describe how these angles change with time. Start with the body frame rates of change with respect to the Euler angles and derivatives as follows.

$$p = \dot{\varphi} - \dot{\psi}\sin\theta \quad (2)$$

$$q = \dot{\theta}\cos\varphi + \dot{\psi}\cos\theta\sin\varphi \quad (3)$$

$$r = \dot{\psi}\cos\theta\cos\varphi - \dot{\theta}\sin\varphi \quad (4)$$

This completes the first block of computer-based simulation (Fig. 7). Given the body angular rates and instantaneous measurements of Euler angles, Euler rates can be calculated. By integrating these Euler rates with respect to time, subsequent Euler angles with respect to current rates and time step can be computed. With these relationships, the orientation can be described. The $\psi - \theta - \varphi$ Euler angles describe the relationship between the inertial frame and the current body fixed reference frame. Additionally, the rates of change of these angles can be determined from the angles themselves and the body fixed angular rates, as can be seen in equations (2– 4). The next task is to compute the body angular rates. These rates can be produced from a set of equations describing the angular dynamics of rigid body.

$$\vec{M} = I\dot{\vec{\omega}} + \vec{\omega}\times(I\vec{\omega}) \quad (5)$$

Where $\vec{\omega}$ is body rate and is equal to: $\vec{\omega} = (p, q, r)$. If the reaction wheel acceleration effects on TSST can be obtained by modeling them as external torques: $M_i = -I_{wi}(\dot{\Omega}_i + \dot{\omega}_i)$, we will derive:

$$\dot{p} = \frac{(I_{yy} - I_{zz})qr}{I_{xx} + I_{wx}} - \frac{I_{wx}\dot{\Omega}_x}{I_{xx} + I_{wx}} \quad (6)$$

$$\dot{q} = \frac{(I_{zz} - I_{xx})pr}{I_{yy} + I_{wy}} - \frac{I_{wy}\dot{\Omega}_y}{I_{yy} + I_{wy}} \quad (7)$$

$$\dot{r} = \frac{(I_{xx} - I_{yy})qp}{I_{zz} + I_{wz}} - \frac{I_{wz}\dot{\Omega}_z}{I_{zz} + I_{wz}} \quad (8)$$

The rates of change of TSST angular velocities with time have been obtained, depending only on the reaction wheels. Its angular velocities can be obtained by integration. Equations (2) – (4) and (6) – (8) formed the main parts of spacecraft simulator dynamics. As seen in these equations, six equations with six states describe the system in the state-space domain [17].

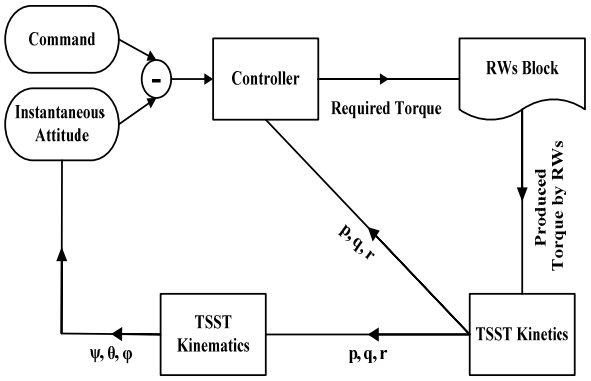

Fig. 7. Schematic of computer-based simulation

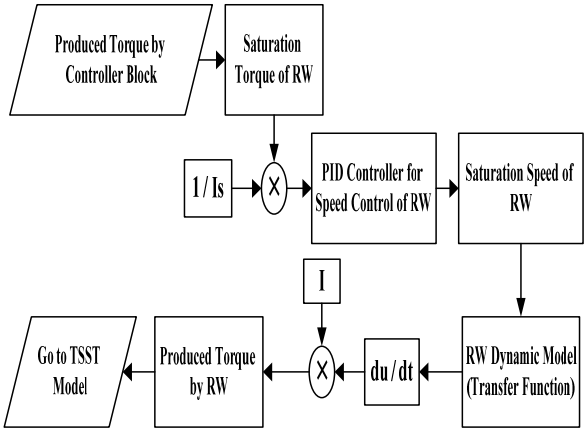

Fig. 8. Schematic of RW block in computer-based simulation

Control

We know that the linear time-invariant state equation [18]

$$\begin{aligned}\dot{x}(t) &= Ax(t) + Bu(t)\\ y(t) &= Cx(t)\end{aligned} \tag{9}$$

represents the open-loop system to be controlled. Our focus is on the application of LQR control laws of the form

$$u(t) = -Kx(t) + Gr(t) \tag{10}$$

In which the reference input is multiplied by a gain G to be chosen so that for a step reference input $r(t) = \beta, t \geq 0$, the output of the closed-loop state equation

$$\begin{aligned}\dot{x}(t) &= (A - BK)x(t) + BGr(t)\\ y(t) &= Cx(t)\end{aligned} \tag{11}$$

satisfies

$$y_{ss} = \lim_{t\to\infty} y(t) = \beta \tag{12}$$

The matrix K must be evaluated under the objective of achieving the best performance index of the form

$$J = \int_0^\infty (x^T Qx + u^T Ru)dt \tag{13}$$

From a frequency-domain viewpoint, the steady-state tracking objective requires that the closed loop transfer function

$$H_{CL}(s) = C(sI - A + BK)^{-1} BG \tag{14}$$

Have what we refer to as identity dc gain; that is, $H_{CL}(0) = I$. For then, with $\beta(s) = \beta(1/s)$ we may apply the final-value theorem to obtain

$$y_{ss} = \lim_{s\to 0} sH_{CL}(s)\beta(1/s) = H_{CL}(0)\beta = \beta \tag{15}$$

The closed-loop dc gain is given by

$$H_{CL}(0) = -C(A - BK)^{-1} BG \tag{16}$$

Thus, if $-C(A-BK)^{-1}B$ is nonsingular, we can achieve identity dc gain by setting

$$G = -\left[C(A - BK)^{-1} B\right]^{-1} \tag{17}$$

As shown in the previous section, the vector of state-space variables is $x = [\psi, \theta, \varphi, p, q, r]^T$ and the vector of control inputs is $u = [\dot{\Omega}_{w1}, \dot{\Omega}_{w2}, \dot{\Omega}_{w3}]^T$.

According to equations (2– 4), (6– 8) and (11), the matrices A and B are:

$$A = \begin{bmatrix} 0 & 0 & 0 & 0 & -s\varphi/c\theta & -c\varphi/c\theta \\ 0 & 0 & 0 & 0 & -c\varphi & s\varphi \\ 0 & 0 & 0 & -1 & -s\varphi s\theta/c\theta & -s\theta c\varphi/c\theta \\ 0 & 0 & 0 & 0 & \dfrac{(I_{yy}-I_{zz})r}{I_{xx}+I_{wx}} & 0 \\ 0 & 0 & 0 & 0 & 0 & \dfrac{(I_{zz}-I_{xx})p}{I_{yy}+I_{wy}} \\ 0 & 0 & 0 & \dfrac{(I_{xx}-I_{yy})q}{I_{zz}+I_{wz}} & 0 & 0 \end{bmatrix}$$

and

$$B = \begin{bmatrix} 0 & 0 & 0 \\ 0 & 0 & 0 \\ 0 & 0 & 0 \\ \dfrac{I_{wx}}{I_{wx}+I_{xx}} & 0 & 0 \\ 0 & \dfrac{I_{wy}}{I_{wy}+I_{yy}} & 0 \\ 0 & 0 & \dfrac{I_{wz}}{I_{wz}+I_{zz}} \end{bmatrix} \tag{18}$$

Now, if we suppose

$$C = \begin{bmatrix} 1 & 0 & 0 & 0 & 0 & 0 \\ 0 & 1 & 0 & 0 & 0 & 0 \\ 0 & 0 & 1 & 0 & 0 & 0 \end{bmatrix} \tag{19}$$

$Q = I(6\times 6)$ and $R = I(3\times 3)$, we can achieve an appropriate matrix K for LQR controller that minimizes the performance index J.

By applying this algorithm, we are able to use LQR algorithm for commanding to the system from a desired initial point to a desired final point.

Figure 9 shows the LQR flowchart applied to system dynamics to achieve appropriate control for commanding testbed.

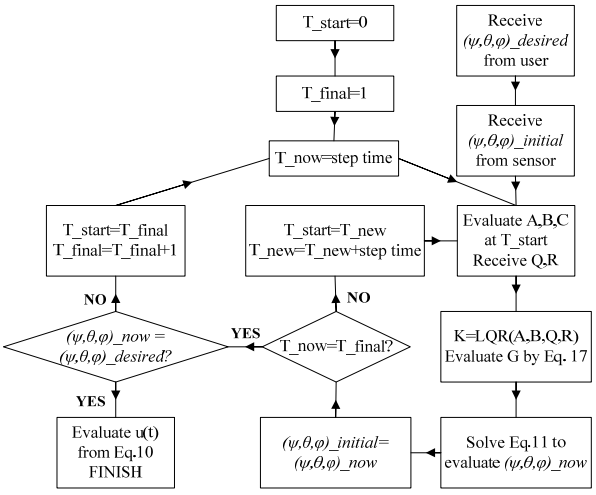

Fig. 9. The LQR flowchart applied to system [19]

To investigate the ability of RWs, a Rapid Control Prototyping (RCP) process has been applied. The block-diagram of RCP process is shown in **Error! Reference source not found.**. In this test, the initial attitude of the system was set to $\lfloor 0^\circ \quad 0^\circ \quad 0^\circ \rfloor$ for yaw, pitch and roll and the desired attitude was set to $\lfloor 20^\circ \quad 10^\circ \quad -10^\circ \rfloor$ Fig. 11. demonstrates the outputs of RCP test. The results of RCP show that the performance of RWs and their internal PID controllers are sufficiently acceptable.

Figure 12 shows a desired maneuver of the system using the proposed control. Also in this figure, a comparison between LQR and PD controllers in the ideal and real conditions has been demonstrated. In the ideal simulation (PD_S), all the perturbation resources except the noise of IMU-AHRS have been neglected and a PD controller has been applied. On the other hand, in the real condition (PD_R) simulation, the perturbation resources such as aerodynamic torques of air-bearing, the offset between center of mass (CM) and center of rotation (CR) and noise of sensor have been considered. To compute the optimal PD coefficients, a Non-dominated Sorting Genetic Algorithm (NSGA-II) has been applied. For this study, two objective functions (energy consumption and agility) and three accuracy constraints have been considered. The general form of optimization can be written as:

$$\begin{aligned} &Minimize\ F = \lfloor F_1 \quad F_2 \rfloor \\ &where \quad F_1 = \left\{ \sum_{n=1}^{N} \sum_{i=x,y,z} \left(\int_0^T \left| u_i(t) \right| dt \right) \right\} \Big/ N, \\ &\qquad F_2 = \left\{ \sum_{n=1}^{N} \sum_{i=x,y,z} \left(\int_0^T \left| e_i(t) \right| dt \right) \right\} \Big/ N, \\ &s.t. \quad C_1 : \mathrm{Re}liability\left\{ \left| e_i(T) \right| < 0.2^\circ \right\} > 0.95, i = x, \end{aligned} \tag{20}$$

In equation (13), N is the number of predefined maneuvers of TSST, u_i is the control effort along ith axis, e_i is the error signal along i^{th} axis and T is the total time of a maneuver. The accuracy constraints have been defined as the reliability of accurate maneuvers being greater than 95%. If the difference between the final point and the desired point about all body axes is less than 0.2, it would be accurate. A esired maneuver of the system has been shown in Fig. 12. Also this figure demonstrates the body rates, control signals and produced torques by RWs for all the three mentioned situations. Because of the saturation of RWs in real condition simulation (in order to consider perturbation resources), the system cannot stay at desired attitude. To correct it, the system should utilize other actuators (such as cold gas thrusters); or the perturbation resources (especially aerodynamic torques of air-bearing and offset between CM and CR) should be sufficiently minimized.

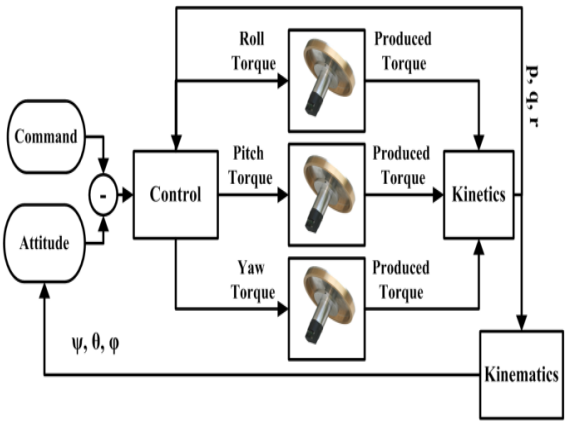

Fig. 10. The schematics of RCP process

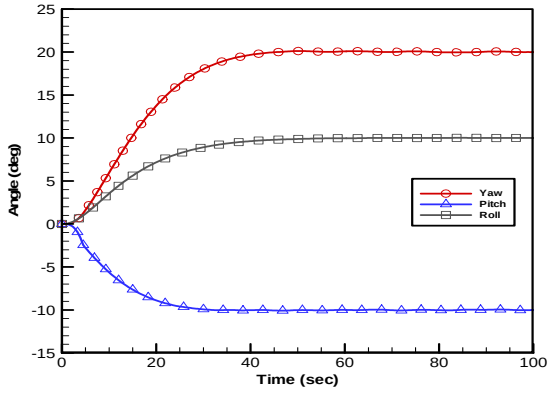

(a)

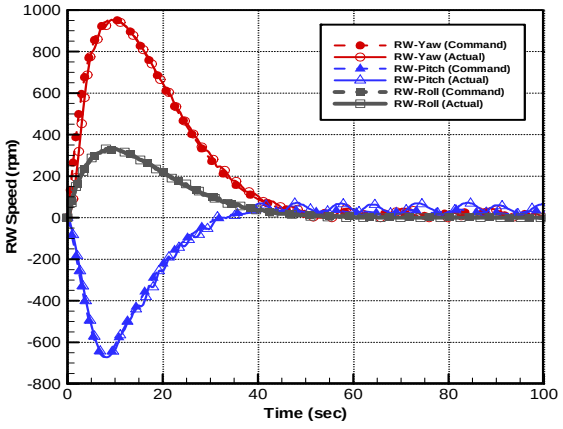

(b)

Fig. 11. The results RCP test, (a) Euler angles, (b) Rws Speed

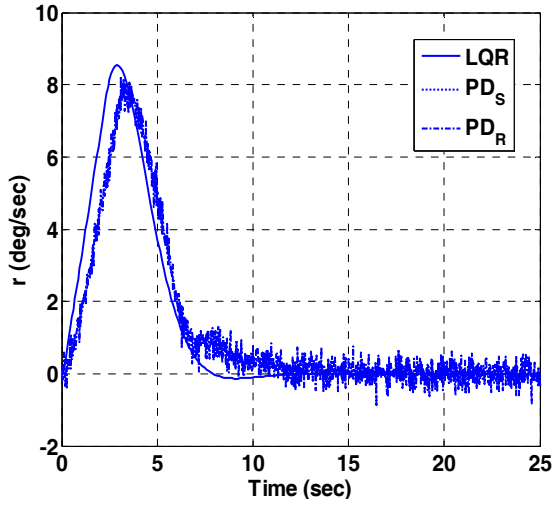
LQR
PD_S
PD_R
r (deg/sec)
Time (sec)

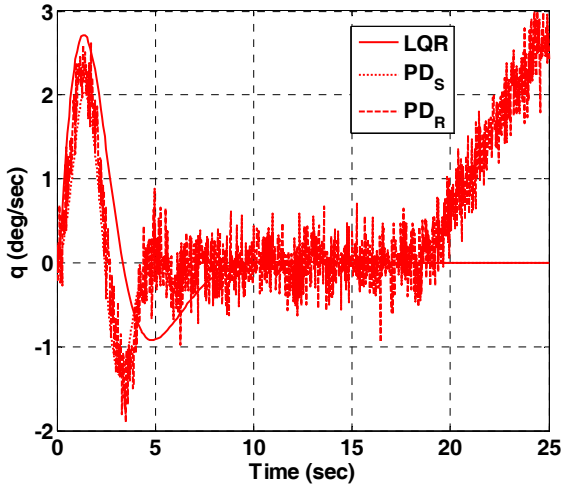
LQR
PD_S
PD_R
q (deg/sec)
Time (sec)

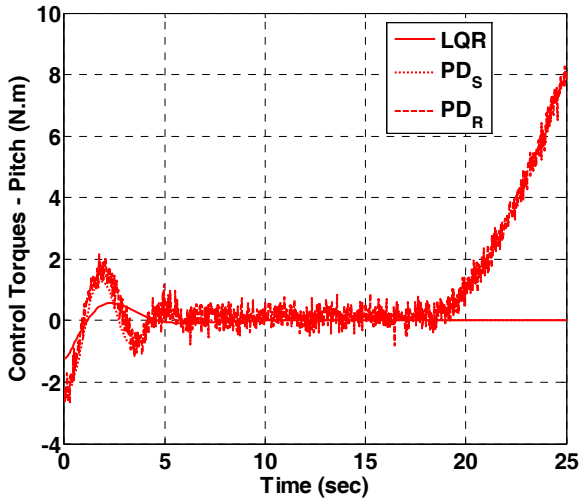
LQR
PD_S
PD_R
Control Torques - Pitch (N.m)
Time (sec)

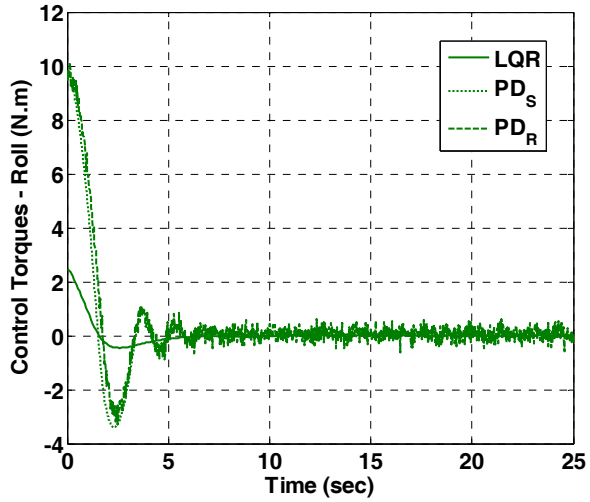
LQR
PD_S
PD_R
Control Torques - Roll (N.m)
Time (sec)

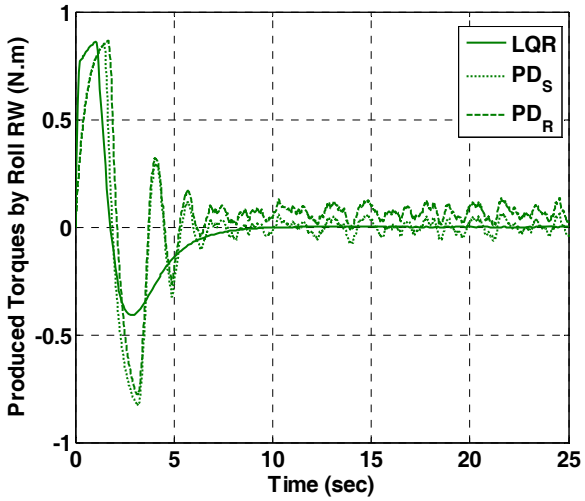
LQR
PD_S
PD_R
Produced Torques by Roll RW (N.m)
Time (sec)

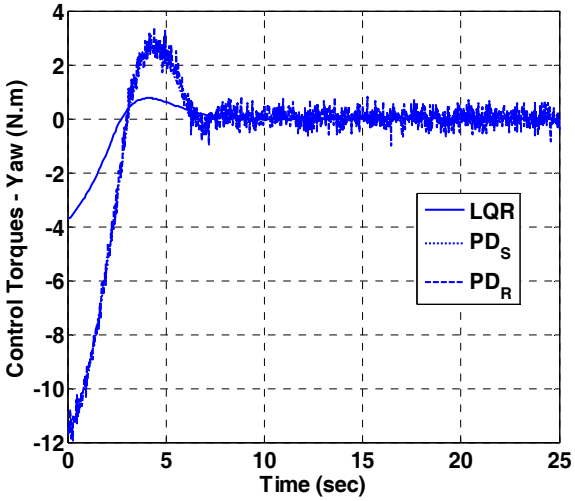
LQR
PD_S
PD_R
Control Torques - Yaw (N.m)
Time (sec)

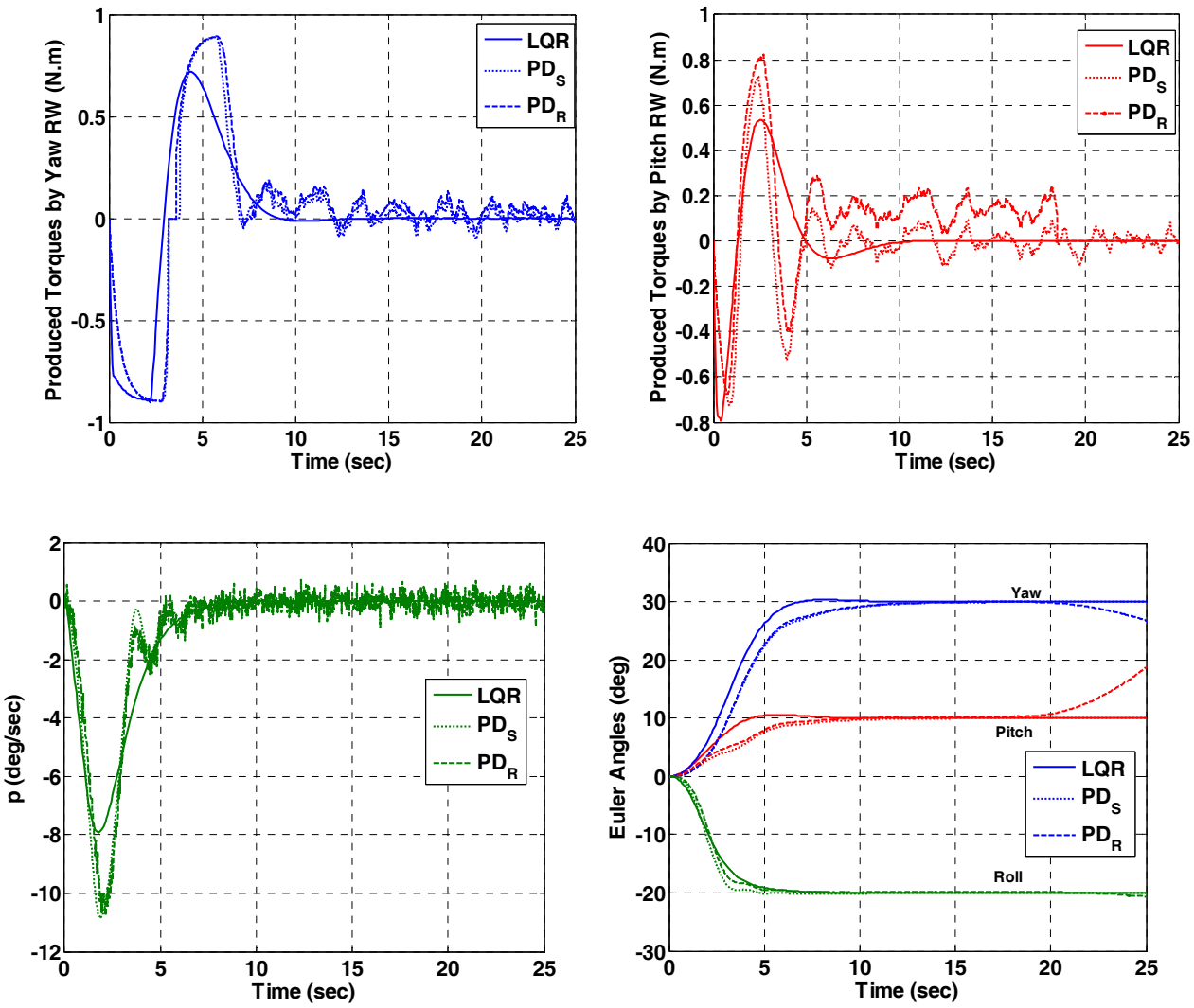

Fig. 12. Euler angles, body rates, control and RW torques (Initial Point: $\varphi = 0°$, $\theta = 0°$, $\psi = 0°$ / Command: $\varphi = -20°$, $\theta = 10°$, $\psi = 30°$)

Conclusion

In this paper, we discussed a tri-axial spacecraft simulator manufactured by our technical team in SRL at K. N. Toosi University of Technology. Also, a spacecraft attitude control algorithm to provide optimal control of a satellite undergoing a large, multi-axis slewing maneuver, given full state feedback was presented. This control algorithm was implemented on the modeling of the spacecraft simulator using reaction wheels as the only control input to validate the results.

References

[1] Kim, B., Velenis, E., Kriengsiri, P. and Tsiotras, P., "Designing a Low-Cost Spacecraft Simulator, *Control Systems," IEEE,* Vol. 23, No. 4, 2003, pp. 26-37.

[2] Schwartz, J. L., Peck, M. A. and Hall, C. D., "Historical Review of Air-Bearing Spacecraft Simulators," *Journal of Guidance, Control, and Dynamics,* Vol. 26, No. 4, 2003, pp. 513-522.

[3] Liu, Y., Zhou, J., Chen, H. and Mu, X., "Experimental Research for Flexible Satellite Dynamic Simulation on Three-Axis Air-Bearing Table," *Proceedings of the Institution of Mechanical Engineers, Part G: Journal of Aerospace Engineering,* Vol. 227, No. 2, 2013, pp. 369-380.

[4] Mirshams, M., Taei, H., Ghobadi, M. and Haghi, H., "Spacecraft Attitude Dynamics Simulator Actuated by Cold Gas propulsion System," *Proceeding of the Institution of Mechanical Engineering, Part G: Journal of Aerospace Engineering,* Vol. 229, No. 8, 2015, pp. 1510-1530.

[5] Prado, J., Bisiacchi, G., Reyes, L., Vicente, E., Contreras, F., Mesinas, M. and Juárez, A., "Three-Axis Air-Bearing Based Platform for Small Satellite Attitude

Determination and Control Simulation," *Journal of Applied Research and Technology,* Vol. 3, No. 3, 2005, pp. 222-237.

[6] Cho, S. and McClamroch, N. H., "Feedback Control of Triaxial Attitude Control Testbed Actuated by Two Proof Mass Devices," *Decision and Control, Proceedings of the Conference on*, USA, 2002, pp. 498-503.

[7] Saulnier, K., Pérez, D., Huang, R., Gallardo, D., Tilton, G. and Bevilacqua, R., "A Six-Degree-of-Freedom Hardware-in-the-Loop Simulator for Small Spacecraft, *Acta Astronautica,*" Vol. 105, No. 2, 2014, pp. 444-462.

[8] Kinnett, R. L., System Integration and Control of a Low-Cost Spacecraft Attitude Dynamics Simulator, (M. Sc. Thesis) Aerospace Engineering, California Polytechnic State University, 2010.

[9] Wilson, W. R., Jones, L. L. and Peck, M. A., "A Multimodule Planar Air Bearing Testbed for CubeSat-Scale Spacecraft," *Journal of Dynamic Systems, Measurement, and Control,* Vol. 135, No. 4, 2013, pp. 1-10.

[10] Li, J., Post, M. A. and Lee, R., "Nanosatellite Attitude Air Bearing System Using Variable Structure Control," *Proceeding of Electrical & Computer Engineering (CCECE),* China, 2012.

[11] Peck, M. A., Miller, L., Cavender, A. R., Gonzalez, M. and Hintz, T., "An Airbearing-Based Testbed for Momentum Control Systems and Spacecraft Line of Sight," *Advances in the Astronautical Sciences,* Vol. 114, 2003, pp. 427-446.

[12] Aghalari, A., Kalhor, S. A., Dehghan, M. M. and Cheheltani, S. H., "Manufacturing and Test of an Attitude Dynamics Simulator for Microsatellites Based on CMG," *Journal of Aerospace Science and Technology,* Vol. 7, No. 3, 2013, pp. 51-67 (In Persian).

[13] Kim, J. J. and Agrawal, B. N., "Automatic Mass Balancing of Air-Bearing-Based Three-Axis Rotational Spacecraft Simulator," *Journal of Guidance, Control, and Dynamics,* Vol. 32, No. 3, 2009, pp. 1005-1017.

[14] Jung, D. and Tsiotras, P., "A 3-dof Experimental Test-Bed for Integrated Attitude Dynamics and Control Research," *AIAA Guidance, Navigation and Control Conference*, USA, 2003.

[15] Mirshams, M., Taei, H. and Vahid, M., A Systems Engineering for Satellite Simulator Design, *ASME Conference on Systems Engineering*, Turkey, 2010.

[16] Sidi, M.J., *Spacecraft Dynamics and Control: A Practical Engineering Approach*, UK: Cambridge University Press, 2000.

[17] Shen, J., McClamroch, N. H. and Bloch, A. M., "Local Equilibrium Controllability of the Triaxial Attitude Control Testbed," *Proceedings of 41st IEEE Conference on Decision and Control*, USA, 2002.

[18] Williams, R. and Lawrence, D., *Linear State-Space Control Systems*, USA: Ohio University, 2007.

[19] Taei, H., *Optimal Design of a Satellite Attitude Motion Simulator*, (M. Sc. Thesis), Aeospace Engineering Faculty, K. N. Toosi University of Technology, 2009 (In Persian).